CrystEngComm

Mechanism of Surface Reaction and Crystal Growth of Cerium Oxide by Supercritical Hydrothermal Treatment with Carboxylic Acids

Journal:	*CrystEngComm*
Manuscript ID	CE-ART-06-2021-000720.R1
Article Type:	Paper
Date Submitted by the Author:	23-Jun-2021

Complete List of Authors:	Omura, Yuki; Tohoku University, Department of Chemical Engineering Yoko, Akira; WPI – Advanced Institute for Materials Research (WPI-AIMR) Tohoku University, Seong, Gimyeong; Tohoku Daigaku, A New Industry Creation Hatchery Center Tomai, Takaaki ; Tohoku University, Institute of Multidisciplinary Research for Advanced Materials Adschiri, Tadafumi; Tohoku Daigaku, New Industry Creation Hatchery Center; Tohoku University, Wpi AIMR; Tohoku Daigaku, Institute of Multidisciplinary Research for Advance Materials

Mechanism of Surface Reaction and Crystal Growth of Cerium Oxide by Supercritical Hydrothermal Treatment with Carboxylic Acids

Yuki Omura[a,b], Akira Yoko[c], Gimyeong Seong[d], Takaaki Tomai[e], Tadafumi Adschiri*[c,d,e]

a: Department of Chemical Engineering, Graduate School of Engineering, Tohoku University, 2-2-1 Katahira, Aoba-ku, Sendai 980-8577, Japan

b: Technical Research Institute, Toppan Printing Co., Ltd., 4-2-3 Takanodai-minami, Sugito-machi, Kita-katsushika-gun, Saitama 345-8508, Japan

c: WPI – Advanced Institute for Materials Research (WPI-AIMR), Tohoku University, 2-1-1 Katahira, Aoba-ku, Sendai 980-8577, Japan

d: New Industry Creation Hatchery Center, Tohoku University, 6-6-10 Aoba, Aramaki, Aoba-ku, Sendai 980-8579, Japan

e: Institute of Multidisciplinary Research for Advanced Materials, Tohoku University, 2-1-1 Katahira, Aoba-ku, Sendai 980-8577, Japan

*: Corresponding author: tadafumi.ajiri.b1@tohoku.ac.jp

Abstract

This study revealed the mechanisms of surface reaction and crystal growth of cerium oxide (CeO_2) by supercritical hydrothermal treatment with carboxylic acids. CeO_2 particles with the average size of 16 nm were hydrothermally treated with decanoic acid in the temperature range of 300–400 °C. The average particle size became over 20 nm with decanoic acid whereas the particle size hardly changed without decanoic acid. Additionally, the octahedral shape of CeO_2 changed to ellipsoid shape after the treatment. Decanoic acid drastically increases the dissolved amount of cerium ion through formation of cerium (III) decanoate. Furthermore, the presence of water promotes reprecipitation of the cerium decanoate to CeO_2 where, cerium (III) decanoate acts as intermediates of dissolution and reprecipitation process. Appropriate amounts of decanoic acid and water accelerate this dissolution–reprecipitation cycle, which promotes particle growth. The higher temperature promotes particle growth because of the increase of the kinetics of complex formation and reprecipitation.

1. Introduction

Demands for high-performance materials have been increasing in many diverse industries. Creating organic–inorganic materials is a promising solution to achieve the required performance. These hybrid materials combine features of organic and inorganic materials.[1,2] Organic materials show flexibility, transparency, and plasticity. Inorganic

materials show mechanical strength, thermal stability, and optical and electrochemical properties. Among inorganic materials, metal oxides exhibit various properties depending on their constituent elements, particle size, and morphology.

Hybridization of these materials is industrially useful. However, metal oxides are generally hydrophilic. Moreover, they have low affinity with organic materials. When the particle size of these oxides become smaller, their surface energy is increased by increased specific surface area, particularly in nanoscale conditions. Metal oxide nanoparticles thus form aggregates, which impairs their original properties. To improve dispersion, organic modification of metal oxides is an effective method. Organically modified particles can disperse while maintaining their primary particle size in organic materials. These composite materials are useful in various applications such as pigments, optical and electrical devices, and nanofluids.[3–6]

Supercritical hydrothermal treatment with organic modifiers is a promising method for synthesizing organically modified metal oxide nanoparticles.[7,8] When the water temperature and pressure change, the properties of water such as density, ionic product, and dielectric constant change accordingly. Particularly, the dielectric constant decreases drastically near the critical point (374 °C, 22.1 MPa) and approaches that of nonpolar molecules.[9,10] Water and organic modifiers therefore form homogeneous phase.

Modifiers can react with metal oxides in a short time on the order of a second.[11,12] Several combinations of organically modified metal oxides with different functional groups in supercritical water have been synthesized, such as carboxylic acid,[13,14] alcohol,[15] and amine[16] modified CeO_2, carboxylic acid modified ZrO_2,[17] Co_3O_4,[18] and HfO_2,[19] and phosphonic acid modified TiO_2.[20] Various factors such as shapes, length, and the grafting density of organic modifiers can affect the nanoparticles polarity and dispersion in organic solvents.

Mechanistic studies of treatments have been reported. Fujii et al. conducted hydrothermal treatment of boehmite (AlOOH) with carboxylic acids.[21–23] The addition of carboxylic acids changed the crystal morphology from rhombic plates to hexagonal plates and increased the particle volume. Those findings suggest the formation of complexes of Al ions and carboxylic acids.[21] Such complexes can facilitate the dissolution of boehmite particles and can enhance the dissolution–recrystallization process. Similarly, Taguchi et al. suggested the formation of complexes during the synthesis of monocarboxylic-acids-modified CeO_2.[13] They synthesized monocarboxylic acids modified CeO_2 from cerium hydroxide. Particles synthesized with carboxylic acids became larger than those without carboxylic acids. They also inferred that intermediates consisting of Ce ion and carboxylic acids changed the solubility. According to these reports, intermediates of metal–organic

complexes might be formed in hydrothermal treatment with organic modifiers. However, the existence and the effects of the intermediate on particle growth have not been verified. Consequently, quantitative investigations of intermediate formation and particle growth must be undertaken.

This study selected CeO_2 and decanoic acid as model compounds to elucidate the mechanism of surface reactions of metal oxides. CeO_2 is used in various applications such as catalysts, polishing agents, gas sensors, and UV-shielding materials; it is sensitive to changes caused by organic modification.[24–27] Earlier studies demonstrated that the size-control and shape-control of particles by high-density modification were possible in supercritical water. Cubic controlled CeO_2 synthesized in supercritical water has high oxygen storage capacity. It is particularly useful for redox catalysts.[28] The study described herein proves experimentally, for the first time ever reported, that decanoic acid brings the Ce dissolution from CeO_2 through formation of a complex, cerium (III) decanoate during modification under supercritical hydrothermal conditions. In addition, the overall reaction and crystal growth mechanism are elucidated.

2. Experimental

2.1. Material

Cerium oxide (CeO_2, Product No. 544841-25G; Aldrich) was used as the raw material. Particles of the raw CeO_2 were measured using X-ray diffraction as 16 nm. Their specific surface area was measured as 38 m^2/g using Brunauer–Emmett–Teller (BET) method using N_2. Decanoic acid (DA), cerium nitrate hexahydrate $Ce(NO_3)_3 \cdot 6H_2O$, sodium decanoate, benzene, methanol, and cyclohexane were purchased from Fujifilm Wako Pure Chemical Corp.

2.2. Hydrothermal treatment

Hydrothermal treatment was performed using a pressure-resistant Hastelloy C vessel (5 mL inner volume). CeO_2, DA and distilled water were loaded into the reaction vessel. Hydrothermal treatment was performed in an electric furnace (AKICO Corp.) for 10–60 min. The DA concentration was changed from 0 to 0.8 (mol/L-vessel) at 400 °C, for 10 min, with 0.5 (kg/L-vessel) water, and 0.05 (mol/L-vessel) of CeO_2. Water density was changed from 0.002 to 0.59 kg/L at 380 °C, for 10 min. Temperature was changed from 300 to 400 °C at 38 MPa. All conditions are presented in Table S1.

After treatment, the vessel was quenched in a room temperature water bath. Then, the products were collected using benzene. After water was removed, methanol was added to the benzene solution. The volume ratio of benzene to methanol was 7:3. CeO_2 particles

precipitated in the benzene–methanol solution and cerium–DA complexes dissolved in the solution. CeO_2 and cerium-DA complexes were separated by centrifugation. The precipitated CeO_2 were washed twice by centrifugation and decantation with benzene–methanol solvents. The washed CeO_2 particles were redispersed in cyclohexane and were freeze dried.

2.3. Extraction process

Cerium–DA complexes were extracted from the benzene–methanol supernatant. The supernatant was evaporated; solid products were obtained. Then, the solids were added to cyclohexane, producing a white turbid solution. The cyclohexane-soluble phase included unreacted DA. The cyclohexane-insoluble chemicals were collected by filtration under reduced pressure and were dried at 70 °C overnight. The chemicals were identified and quantified with further analysis.

2.4. Synthesis of cerium (III) decanoate

For comparison, cerium (III) decanoate (Ce (III) decanoate) was synthesized by metathesis reaction. After 0.1 M cerium nitrate aqueous solution and 0.3 M sodium decanoate aqueous solution were prepared, sodium decanoate solution was added to

cerium nitrate solution under stirring at room temperature. The solution was stirred for 30 min. The products were centrifuged and washed using water and ethanol, followed by drying at 70 °C overnight. The infrared adsorption spectrum is consistent with the cerium-carboxylate complex described in an earlier report.[29]

2.5. Characterization methods

Using SmartLab 9MTP (Rigaku Corp.) equipped with a Cu Kα (λ=1.5418 Å) radiation source, the XRD patterns of the products were recorded. The 2θ scan speed was set to 3 °/min. The crystallite sizes of the products were ascertained based on the full width at half maximum (FWHM) of the peaks according to the following Scherrer equation.

$$D = \frac{K\lambda}{\beta\cos\theta} \quad (1)$$

where D is the crystallite size, K is the Scherrer prefactor (typically 0.9), β is the FWHM of the diffraction peak.

The strain effects ε of the products were verified using the following Halder–Wagner equation.[30]

$$\left(\frac{\beta^*}{d^*}\right)^2 = \frac{K\ \beta^*}{D(d^*)^2} + (2\ \varepsilon)^2 \quad (2)$$

$$\beta^* = \frac{\beta\cos\theta}{\lambda} \quad (3)$$

$$d^* = \frac{2\sin\theta}{\lambda} \quad (4)$$

Equation (2) can be rewritten as

$$\left(\frac{\beta}{\tan\theta}\right)^2 = \frac{K\lambda}{D}\left(\frac{\beta}{\tan\theta\sin\theta}\right) + 16\varepsilon^2 \quad (5)$$

From equation (5), $(\beta/\tan\theta)^2$ is plotted against $\beta/(\tan\theta\sin\theta)$. The slope affords $K\lambda/D$.

Fourier-transform infrared (FT-IR) spectra were recorded using an infrared spectrometer (FT/IR-4200; JASCO Corp.). The analytical samples were prepared using KBr method. Thermogravimetric analysis (TGA) was performed using a thermogravimetric analyzer (DTG-60AH; Shimadzu Corp.) with N_2 (99.9999%) carrier gas and a 50 mL/min flow rate. The temperature was first increased to 150 °C and held 1 h to remove adsorbed water, then raised to 750 °C at 10 °C/min. Using a monochromatic Al Kα source, XPS spectra were obtained (PHI5000 Versa Probe II; ULVAC-PHI Inc.). Morphologies of the respective products were observed using transmission electron microscopy (TEM, H-7650; Hitachi High-Technologies Corp.). Inductively coupled plasma atomic emission spectroscopy (ICP-AES) was performed (ARCOS FHM22 MV130; Spectro Analytical Instruments, Ametek Inc.). The cerium ion dissolved as cerium-DA complexes in benzene–methanol solvents and that concentration was measured using ICP-AES. Grafting density of the DA on CeO_2 was calculated according to a method described earlier in the literature.[21] It was calculated using information from TGA weight loss,

particle volume and surface area evaluated by TEM, regarding the shape of the particles as ellipsoids. The OSC was measured using a catalyst characterization analyzer (BELCAT II; MicrotracBEL) at 500 °C. Each sample was reduced for 2 h using hydrogen gas (99.999%) at 500 °C. Then O_2 pulse (99.999%) was introduced at the same temperature. The unreacted O_2 gas was detected with TCD (carrier gas: He, 99.999%). The total amount of consumed O_2 was evaluated by integrating the consumed amount of O_2 at each pulse peak.

3. Results and Discussion

3.1. Particle growth of CeO_2

Figure 1(a) shows TEM images of the untreated CeO_2 (Ut-CeO_2) and CeO_2 treated hydrothermally with DA (DA-CeO_2). Figure 1 shows DA-CeO_2 with 0.045 mol/L DA concentration at 400 °C for 10 min as a representative. Images of other samples are presented in Figure S1. The DA-CeO_2 particles were larger than Ut-CeO_2, which shows that the particles size increased through hydrothermal treatment with DA. These phenomena were confirmed through crystallite size evaluation using XRD analysis (Figure 1b). DA addition increased the XRD crystallite size. The particle size was increased by increasing DA concentration until 0.015 mol/L DA concentration. When the

concentration exceeded 0.015 mol/L, the particle size remained constant. Figure S2 portrays the XRD patterns.

The morphologies before and after the treatment clearly differ. In the TEM images, Ut-CeO_2 has a mostly octahedral structure, whereas DA-CeO_2 has a nearly ellipsoid structure because carboxylic acids can adsorb on {100} facets selectively and reduce the crystal growth rate in the {100} direction. Reportedly, cubic CeO_2 nanoparticles have been synthesized using this mechanism.[8,13,31] In this study, the growth of the {100} facets of the octahedron are apparently suppressed by the DA modification and growth of the {111} planes resulted in elliptical shape.

Figure 2 presents water density effects on particle growth. The higher the water density becomes, the larger the crystallite size becomes. The TEM image depicted in Figure 2(a) demonstrates the particle size difference. Almost no small particles smaller than 10 nm was observed after treatment with higher water density, which indicated particle growth, whereas particles smaller than 10 nm were observed after treatment with lower water density. The XRD particle size, shown in Figure 2(b), also shows a tendency by which the higher water density increases the CeO_2 particle size.

Effects of the hydrothermal treatment temperatures on the particle growth were investigated at 300, 340, and 400 °C (presented in Table S1). Figure 3 shows the relation

between the temperature and XRD crystallite size. Without DA (Figure 3a), particle growth was slow at all temperatures. The difference in crystallite size at different treatment temperatures was negligible, whereas with DA (Figure 3b), the differences between temperatures were large. Particle growth was promoted at the higher temperatures. At 400 °C, the particle size increased over 20 nm during the first 10 min. In contrast, the particle size increased gradually at 300 °C. Carboxylic acids promote CeO_2 particle growth. The water density and the treatment temperature also affect particle growth.

3.2. Organic modification of CeO_2

Figure 4 shows IR spectra of the products. The spectra of DA-CeO_2 differ from the spectrum of Ut-CeO_2, which indicated surface modification. Bands in the region of 2700–3100 cm^{-1} are attributable to the modified DA. A band at 2959 cm^{-1} is assigned to the asymmetric stretching mode of -CH_3. Bands at 2874 cm^{-1} and 2852 cm^{-1} are assigned respectively to the asymmetric and symmetric stretching modes of -CH_2-. No band related to the free carboxyl group (-COOH) of the original DA (normally detected at about 1700 cm^{-1}) was observed in the spectra of the products, indicating that unmodified DA was washed away from the products. Bands at 1534 cm^{-1} and 1438 cm^{-1} are assigned to the

asymmetric and symmetric modes of carboxylate (COO^-). Thereby, DA strongly combines with CeO_2 through carboxylate groups.[13,32]

Figure 5 shows the product TGA curves. The weight loss of the Ut-CeO_2 between 150–750 °C was 0.54% including the water and oxygen contents inside the lattice. Therefore, the weight loss originated from modified DA was estimated by deducting that of Ut-CeO_2. The weights of DA-CeO_2 decreased drastically from 350 to 450 °C, which was derived from thermal decomposition of the DA modifier. The weight loss occurred at a higher temperature than DA boiling point (270 °C), which demonstrates stable carboxylate bonds of the DA on CeO_2. Figures 6(a) and (b) show effects of DA and water on the grafting density. The higher carboxylic acid concentration and the lower water density increased grafting density. Carboxyl groups combine with surface hydroxyl groups, probably through a dehydration reaction as presented below.

$$Ce\text{-}(OH)_x + yCH_3(CH_2)_8COOH \leftrightarrows Ce\text{-}(OH)_{x-y}(OOC(CH_2)_8CH_3)_y + yH_2O \quad (a)$$

Results of the Figures 6(a) and (b) are explainable by consideration of the reaction above: the higher carboxylic acid concentration and the lower water density are favorable for high grafting density.

Figures 4 and 5 show that DA combines with CeO_2 surface strongly and it is well known that organic ligands can cap the growing surface and suppress particle growth.[33,34] However, particle growth was promoted through hydrothermal treatment with surface modifier even though the CeO_2 surface was modified stably. Fujii et al. reported similar results that carboxylic acid promotes AlOOH particle growth.[21] They suggested the formation of complexes of Al ions and carboxylic acids. Such complexes can facilitate the dissolution of boehmite particles. However, the existence of the complexes and the structure has not yet been clarified. This report is made on the assumption that the cerium decanoate was synthesized through the treatment. It was extracted from the benzene–methanol supernatant in the following section.

3.3. Analysis of the extracted chemicals

To elucidate the surface reaction mechanisms, chemicals were extracted from DA-CeO_2 after hydrothermal treatment (sec. 2.3). Figure 7 shows IR spectra of the extracted chemicals, which corresponded with that of Ce (III) decanoate synthesized as reference (sec. 2.4). Bands at 1532 cm^{-1} and 1453 cm^{-1} are assigned respectively to the asymmetric and symmetric modes of carboxylate (COO^-). Asymmetric mode was found to have higher absorbance than that of symmetric mode, indicating that it is carboxylate-bond

with cerium ions.[35] No band related to the Ce–O of the CeO_2 (normally detected at about 500 cm^{-1}) was observed in the spectra of the extracted chemicals.

The extracted chemicals and Ce (III) decanoate were also compared in the XPS spectrum, as shown in Figure 8. The XPS spectrum of the extracted chemicals corresponded with that of Ce (III) decanoate. No band related to the Ce^{4+} (916 eV) was observed in the spectra of the extracted chemicals and Ce (III) decanoate, which indicates that extracted chemicals are trivalent complexes.[36] Table S2 presents the atomic concentration from the XPS spectra. Particularly at the surface, CeO_2 has oxygen vacancies and easily changes the electric charge between Ce^{4+} and Ce^{3+} reversibly. Probably, trivalent Ce on the CeO_2 surface dissolves as complexes. Trivalent Ce (III) complexes reportedly are monomeric, with three decanoate combining with one Ce.[37] These complexes become CeO_2 after TGA measurement. The calculated weight loss is 73.7%. The experimentally obtained weight loss of the Ce (III) decanoate synthesized by metathesis reaction was 72.7% (Figure S3), which corresponds to the calculated weight loss. That finding indicates that Ce (III) decanoate formed in this report is monomeric.

3.4. Measurement of the Ce solubility as complexes

To measure the Ce ion concentration in the benzene-methanol supernatant, ICP-AES

was applied. The Ce ion concentration reveals the amount of dissolved Ce ions as complexes during the hydrothermal treatment. Figure 9(a) shows effects of the DA concentration on the CeO_2 dissolution amount. The dissolution amount increased as the DA concentration increased. DA not only reacts with surface hydroxyl group of Ce; it also reacts with surface-modified Ce. When DA reacts with surface modified Ce ($(DA)_2Ce$-O-), the reaction breaks the Ce-O bond of $(DA)_2Ce$-O- on the surface. Through this reaction, DA and $(DA)_2Ce$-O- form Ce (III) decanoate. Considering that mechanism, one can infer that both the grafting density (concentration of $(DA)_2Ce$-O-) and DA concentration in the solvent affect the Ce dissolution rate and the complexes' concentration. The grafting density was changed by changing DA concentration (Figure 6). Consequently, the grafting density was divided from the dissolution amounts and the revised dissolution amounts, as shown in Figure 9(b). Results clarified that DA shifts the reaction equilibrium to the complexes' formation side.

Figure 9(c) shows water density effects on the CeO_2 dissolution. The dissolution amounts, as complexes, decreased as the water density increased. Water can hydrolyze with the complexes to form hydroxides. These hydroxides dehydrated and condensed with CeO_2 crystals. Consequently, the total reaction equilibrium shifts to the CeO_2 side as the water density increases. In addition, reaction equilibrium of the reaction (a) is

shifted to the left side, which retards the Ce dissolution. Both reactions reduce the concentrations of the complexes.

Figure 9(d) presents the effects of temperature and treatment time on the Ce ion dissolution amount. At 300 °C, the dissolution amount was less than 340 and 400 °C at 7 and 10 min. The dissolution amount increased for up to 60 min only at 300 °C. The dissolution rate was accelerated with increased temperature. The kinetics of the dissolution through complexes is lower at 300 °C.

At 400 °C, the dissolution amount was the highest at 7 min. It then decreased. At 340 °C, the dissolution amount increased until 30 min and then decreased. Particle growth and change of the particle shape might reduce the Ce ion dissolution amount (Figure 1, Figure S1). Figure 3(b) shows that the particle growth rate decreased from 30 min to 60 min at 340 and 400 °C. That decrease might be attributable to exposure of the stable {100} facets and reduction of the Ce ion dissolution amount. The particle shape change was also detected using OSC measurements (Table S3). The OSC became higher because of the treatment and longer treatment time. CeO_2 crystals with cubic {100} facets show higher OSC than irregularly shaped cerium crystals.[28] This result therefore indicates the particle shape change and exposure of the {100} facets. The dissolution as the complexes was therefore reduced.

3.5. Mechanisms of surface reaction and crystal growth

Figure 1 shows that DA promotes particle growth. When treated without decanoic acid at 400 °C for 10 min, the particle size was 16.5 nm. When treated with decanoic acid, the particle size was more than 19 nm. The total Ce ion amount remained unchanged; thus, particles grew through Ostwald ripening, by which small particles and the unstable surface dissolved and reprecipitated on large particles. For DA concentration of 0.015 mol/L, the Ce dissolution amount was 1.1×10^{-4} mol/L (Figure 9), whereas the Ce dissolution amount without DA was 1.0×10^{-11} mol/kg in water (300 °C). This solubility was calculated using OLI simulation software (OLI Analyzer 10.0, OLI Systems Inc.). Considering the decrease in the dielectric constant near the critical point, the Ce ion dissolution amount at 400 °C can be expected to be lower than that of 300 °C.[38] DA drastically raised Ce ion solubility through formation of complexes. This increase in solubility can promote Ostwald ripening. However, when carboxylic acid and metal oxides are thermally treated without water, metal oxides reportedly dissolve completely at once.[39] Figure 7(a) also shows that high- speed particle growth requires water. Probably, water accelerates particle growth by promoting the precipitation of the complexes on the CeO_2 surface. Consequently, lower water density suppresses precipitation and restrains

the particle growth. Particle growth requires both DA and water. Figure 1b shows the particle size as constant by changing the DA concentration when the concentration exceeded 0.015 mol/L. The dissolution kinetics can be expected to increase by increasing the DA concentration. However, the reprecipitation kinetics can be expected to decrease by increased DA concentration. Their effects control particle growth.

Scheme 1 portrays the surface reaction and particle growth mechanisms of the CeO_2 and DA estimated from this study. First, carboxyl groups combine with surface hydroxyl groups in a dehydration reaction (surface modification). The higher carboxylic acid concentration and the lower water density are regarded as favorable for high grafting density. After the surface modification reaction, dissolution of Ce ion as the complexes occurs on the modified CeO_2 surface (complexation). Water can hydrolyze with the complexes to form hydroxides $Ce(OH)_{3-z}(OOCR)_z$ (hydroxylation). These hydroxides dehydrate and condense with CeO_2 crystals (reprecipitation). Repeating this cycle promotes particle growth. Appropriate amounts of carboxylic acid and water are required for increasing these complexation, hydroxylation, and reprecipitation reaction rates.

Figure 3 portrays the higher temperature promote particle growth. Figure 9(d) shows that higher temperatures increase the Ce dissolution kinetics. The higher temperature increases the dissolution rate, and probably the reprecipitation rate. The higher

temperature thereby promotes particle growth.

4. Conclusion

Reaction of CeO_2 and decanoic acid and its effects on particle growth were investigated during supercritical hydrothermal treatment. This study extracted and quantified the complexes formed as the intermediates during the treatment. The role of the complex was clarified for precise control of the particle size and shape. Not only do surface modification reactions occur on the CeO_2 surface: dissolution of Ce ions as complexes occurs as well. The reaction increases the Ce ion dissolution amount. Water hydroxylates the complexes and precipitates these complexes on CeO_2 particles. Particle growth is therefore promoted by carboxylic acids and water. The particle growth mechanism would be applicable to control the particle sizes, shapes, and facets of other various metal oxides with further investigations.

Author Contributions

Yuki Omura; Conceptuaelization, methodology, investigation, writing–original draft. Akira Yoko; Conceptualization, methodology, writing–review & editing. Gimyeoug Seong; Investigation, writing–review & editing. Takaaki Tomai; Conceptualization,

investigation, writing–review & editing. Tadafumi Adschiri; Conceptualization, supervision, funding acquisition, writing–review & editing.

Conflicts of interest

There are no conflicts to declare.

Acknowledgments

This study was supported by grants from the Japan Society for the Promotion of Science (JSPS), KAKENHI (Grant Number JP16H06367), New Energy and Industrial Technology Development Organization (NEDO), the Japan Science and Technology Agency (JST) [MIRAI; Grant Number JPMJMI17E4 and CREST, Grant Number JPMJCR16P3], Materials Processing Science Project (Materealize; Grant Number JPMXP0219192801), Core Research Cluster for Materials Science, and World Premier International Research Center Initiative – Advanced Institute for Materials Research (WPI-AIMR), Tohoku University, established by the WPI, Ministry of Education, Culture, Sports, Science and Technology (MEXT), Japan.

References

1 S. H. Mir, L. A. Nagahara, T. Thundat, M.-T. Parvaneh, H. Furukawa, A. Khosla, *J. Electrochem. Soc.*, 2018, **165** (8), B3137–B3156.

2 S. Kango, S. Kalia, A. Celli, J. Njuguna, Y. Habibi, R. Kumar, *Prog. Polym. Sci.*, 2013, **38**, 1232–

1261.

3 D. Rangappa, T. Naka, A. Kondo, M. Ishii, T. Kobayashi, T. Adschiri, *J. Am. Chem. Soc.*, 2007, **129**, 11061–11066.

4 K. Kanie, A. Muramatsu, *J. Am. Chem. Soc.*, 2005, **127**, 11578–11579.

5 P. Kim, N. M. Doss, J. P. Tillotson, P. J. Hotchkiss, M.-J. Pan, S. R. Marder, J. Li, J. P. Calame, J. W Perry, *ACS Nano*, 2009, **3** (9), 2581–2592.

6 D. S. Saidina, M. Z. Abdullah, M. Hussin, *J. Mater. Sci.: Mater. Electron.*, 2020, **31**, 4381–4398.

7 B. J. Zhang, S. Ohara, M. Umetsu, T. Naka, Y. Hatakeyama, T. Adschiri, *Adv. Mater*., 2007, **19**, 203–206.

8 T. Mousavand, S. Takami, M. Umetsu, S. Ohara, T. Adschiri, *J. Mater. Sci*., 2006, **41**, 1445–1448.

9 A. Yoko, G. Seong, T. Tomai, T. Adschiri, *Kona Powder Part. J.*, 2020, **37**, 28–41.

10 D. P. Fernández, Y. Mulev, A. R. H. Goodwin, J. M. H. Levelt Sengers, *J. Phys. Chem. Ref. Data*, 1995, **24** (1), 33–69.

11 J. Lu, K. Minami, S. Takami, M. Shibata, Y. Kaneko, T. Adschiri, *ACS Appl. Mater. Interfaces*, 2012, **4**, 351–354.

12 M. D. de Tercero, I. Gonzáles Martínez, M. Herrmann, M. Bruns, C. Kübel, S. Jennewein, U. Fehrenbacher, L. Barner, M. Türk, *J. of Supercrit. Fluids*, 2013, **82**, 83–95.

13 M. Taguchi, N. Yamamoto, D. Hojo, S. Takami, T. Adschiri, T. Funazukuri, T Naka, *RSC Adv*., 2014, **4**, 49605–49613.

14 T. Arita, J. Yoo, Y. Ueda, T. Adschiri, *Chem. Lett*., 2012, **41**, 1235–1237.

15 B. Giroire, C. Slostowski, S. Marre, C. Aymonier, T. Aida, D. Hojo, N. Aoki, S. Takami, T. Adschiri, *Phys. Chem. Chem. Phys*., 2016, **18**, 1727–1734.

16 A.-A. Litwinowicz, S. Takami, S. Asahina, X. Hao, A. Yoko, G. Seong,; T. Tomai, T. Adschiri, *CrystEngComm*, 2019, **21**, 3836–3843.

17 M. Taguchi, S. Takami, T. Adschiri, T. Nakane, K. Sato, T. Naka, *CrystEngComm*, 2012, **14**, 2132–2138.

18 T. Mousavand, T. Naka, K. Sato, S. Ohara, M. Umetsu, S. Takami, T. Nakane, A. Matsushita, T. Adschiri, *Physical Review B*, 2009, **79**, 144411.

19 S. M. García Montes, S. Takami, M. Goto, R. M. Ibarra, *Nano-Struct. Nano-Objects*, 2020, **24**, 100540-

20 T. Arita, K. Moriya, T. Yoshimura, K. Minami, T. Naka, T. Adschiri, *Ind. Eng. Chem. Res*., 2010, **49**, 9815–9821.

21 T. Fujii, S. Kawasaki, A. Suzuki, T. Adschiri, *Cryst. Growth Des*., 2016, **16**, 1996–2001.

22 T. Fujii, S. Kawasaki, T. Adschiri, *J. of Supercrit. Fluids*, 2016, **118**, 148–152.

23 T. Fujii, S. Kawasaki, M. Kanakubo, *J. of Supercrit. Fluids*, 2017, **119**, 81–87.

24 R. Si, M. Flytzani-Stephanopoulos, *Angew. Chem*., 2008, **120**, 2926–2929.

25 J. Murata, K. Yodogawa, K. Ban, *Int. J. Mach. Tools Manuf.*, 2017, **114**, 1–7.

26 D. E. Motaung, G. H. Mhlongo, P. R. Makgwane, B. P. Dhonge, F. R. Cummings, H. C. Swart, S. S. Ray, *Sens. Actuators B*, 2018, **254**, 984–995.

27 F. Caputo. M. De Nicola, A. Sienkiewicz, A. Giovanetti, I. Bejarano, S. Licoccia, E. Traversa, L. Ghibelli, *Nanoscale*, 2015, **7**, 15643–15656.

28 J. Zhang, H. Kumagai, K. Yamamura, S. Ohara, S. Takami, A. Morikawa, H. Shinjoh, K. Kaneko, T. Adschiri, A. Suda, *Nano Lett*., 2011, **11**, 361–364.

29 K. N. Mehrotra, R. K. Shukla, M. Chauhan, *Bull. Chem. Soc. Jpn*., 1995, **68**, 1825–1831.

30 N. C. Halder, C. N. J. Wagner, *Adv. X-Ray Anal*., 1966, **9**, 91–102.

31 T. Taniguchi, T. Watanabe, N. Sakamoto, N. Matsushita, M. Yoshimura, *Cryst. Growth Des.*, 2008, **8** (10), 3725–3730.

32 L. Zhang, R. He, G. Hong-Chen, *Appl. Surf. Sci.*, 2006, **253**, 2611–2617.

33 K. J. Ziegler, R. C. Doty, K. P. Johnston, B. A. Korgel, *J. Am. Chem. Soc*., 2001, **123**, 7797–7803.

34 T. Togashi, H. Hitaka, S. Ohara, T. Naka, S. Takami, T. Adschiri, *Mater. Lett.*, 2010, **64**, 1049–1051.

35 C. Liu, F. Su, J. Liang, P. Huang, *Surf. Coat. Technol.*, 2014, **258**, 580–586.

36 E. Bêche, P. Charvin, D. Perarnau, S. Abanades, G. Flament, *Surf. Interface Anal*., 2008, **40**, 264–267.

37 A. Sen, H. A. Stecher, A. L. Rheingold, *Inorg. Chem*., 1992, **31**, 473–479.

38 K. Sue, Y. Hakuta, R. L. Smith, Jr., T. Adschiri, K. Arai, *J. Chem. Eng. Data*, 1999, **44**, 1422–1426.

39 K. Zhao, Z. Yang, H. Wei, J. Guo, Y. Yang, J. Wei, *CrystEngComm*, 2020, **22**, 4790–4796.

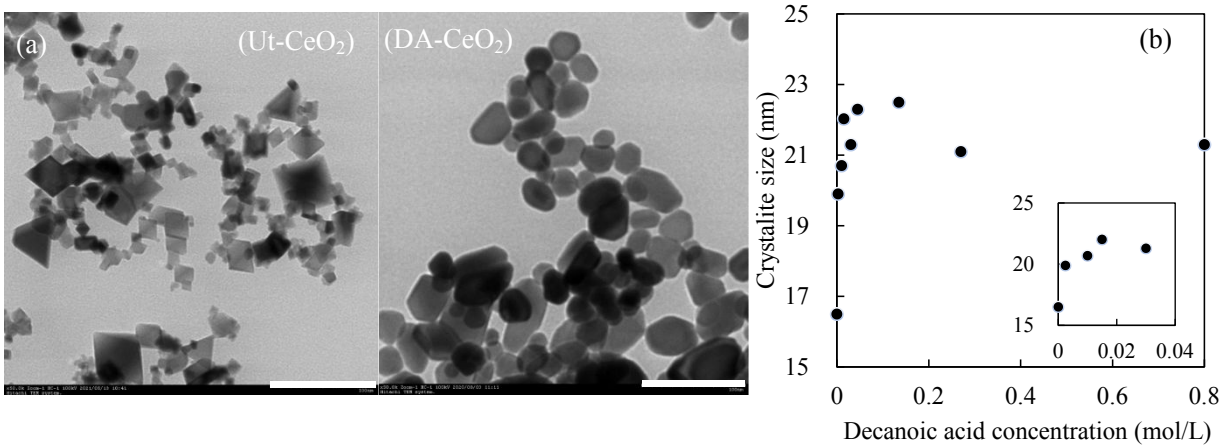

Figure 1. Particle growth of samples.
(a) TEM images of samples. Untreated CeO_2 (Ut-CeO_2) and decanoic acid modified CeO_2 (DA-CeO_2) with 0.045 mol/L DA concentration.
400 °C, 38 MPa, and 0.5 kg/L water density for 10 min.
Scale bars represent 100 nm.
(b) Effects of DA acid concentration on XRD particle size. Inset shows the low range of the decanoic acid concentration 0–0.04 (mol/L)

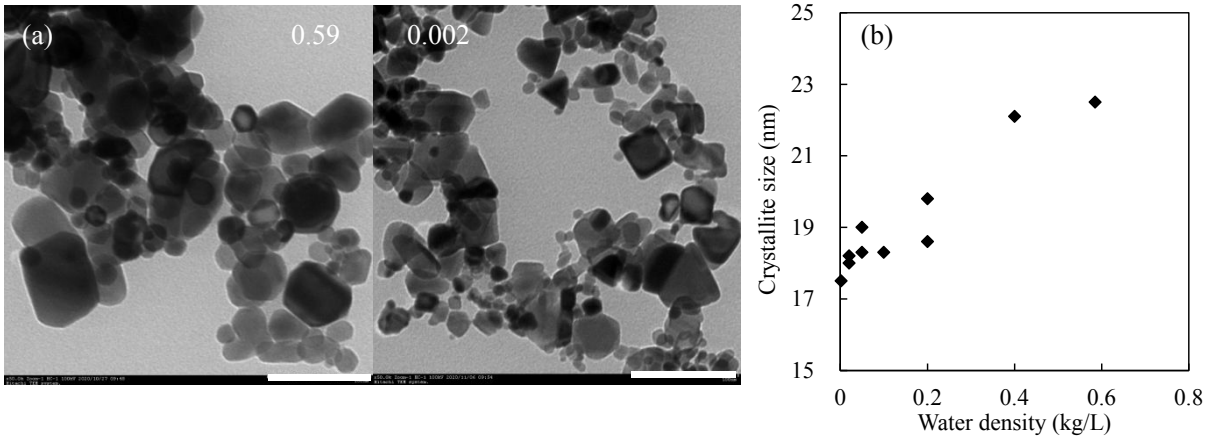

Figure 2. Effects of water density on the particle growth.
(a) TEM images of water density 0.59 and 0.002 kg/L.
0.16 mol/L DA concentration, and 0.06 mol/L CeO_2 concentration, 380 °C for 10 min.
Scale bars represent 100 nm.
(b) XRD particle size.

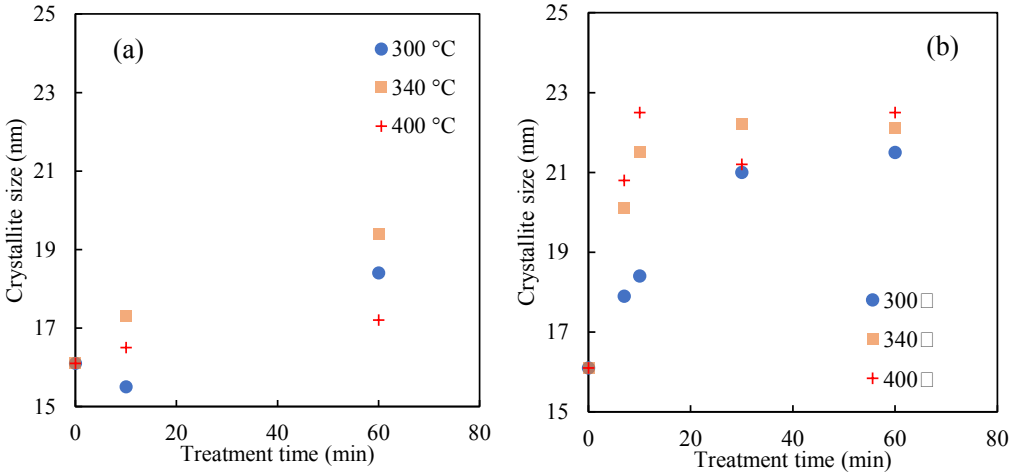

Figure 3. Effects of temperature and decanoic acid concentration on particle size.
38 MPa for 10 min.
(a) Treated without DA.
(b) Treated with DA. The molar ratios of DA and CeO_2 were 2.7:1 at all temperatures.

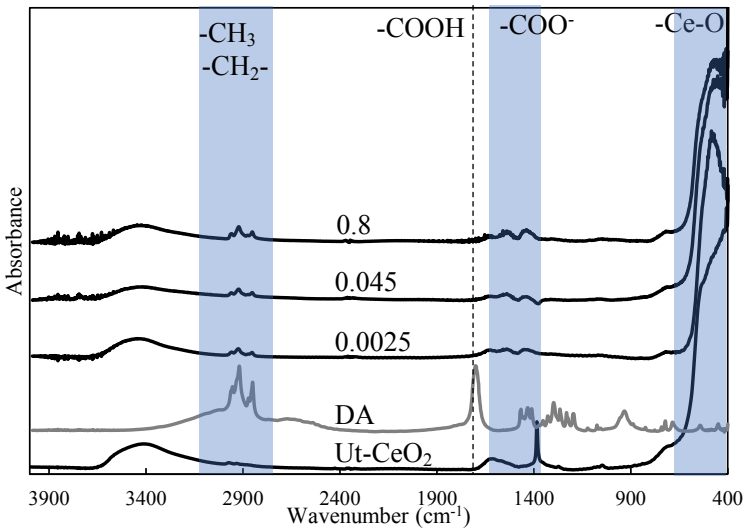

Figure 4. IR spectra of the products. Untreated CeO_2 (Ut-CeO_2), untreated DA, and DA-CeO_2 with 0.0025, 0.045, and 0.8 mol/L DA concentration.
0.05 mol/L CeO_2, 400 °C, and 0.5 kg/L water density for 10 min.

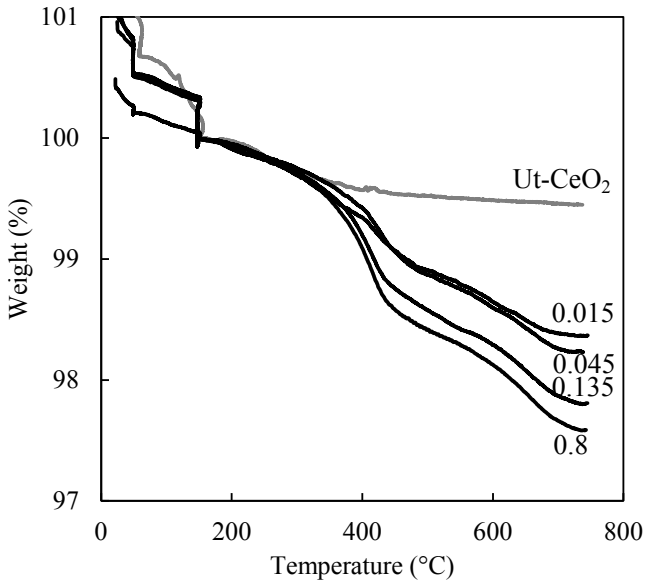

Figure 5. TGA curves of the products. Untreated CeO_2 (Ut-CeO_2), and DA-CeO_2 with 0.015, 0.045, 0.135, and 0.8 mol/L DA concentration.
0.05 mol/L CeO_2, 400 °C, and 0.5 kg/L water density for 10 min.

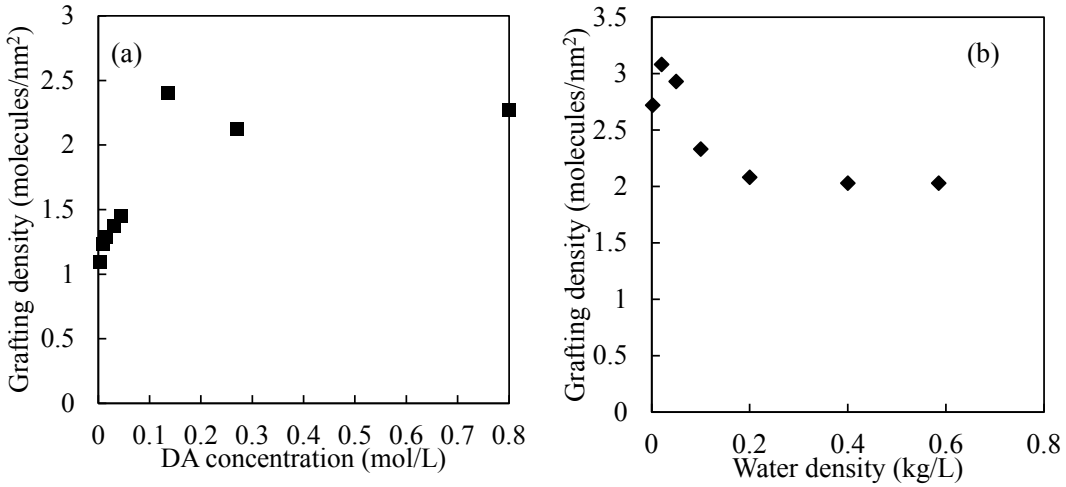

Figure 6. Effects of DA concentration and water density on grafting density.
(a) Effects of DA at 400 °C, 38 MPa, and 0.05 mol/kg CeO_2 concentration for 10 min.
(b) Effects of water at 380 °C, 0.16 mol/L DA concentration, and 0.06 mol/L CeO_2 concentration.

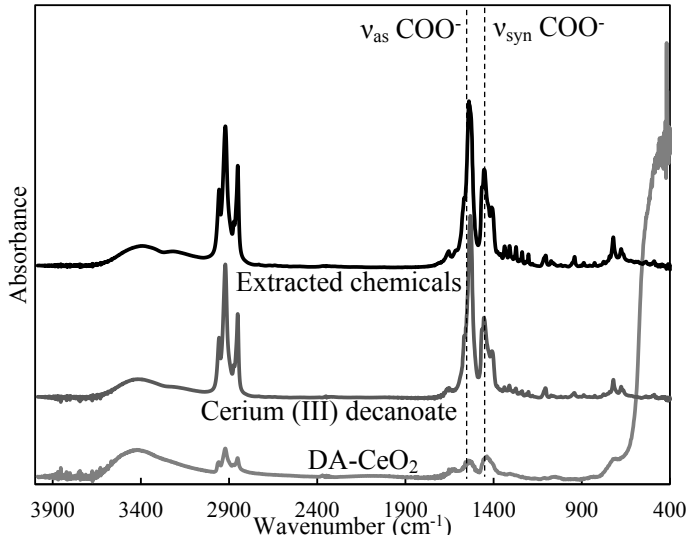

Figure 7. IR spectra of the DA-CeO_2, Ce (III) decanoate, and extracted chemicals. Extraction is performed on the sample 0.8 mol/L DA concentration in water. 0.05 mol/L CeO_2, 400 °C, and 0.5 kg/L water density for 10 min.

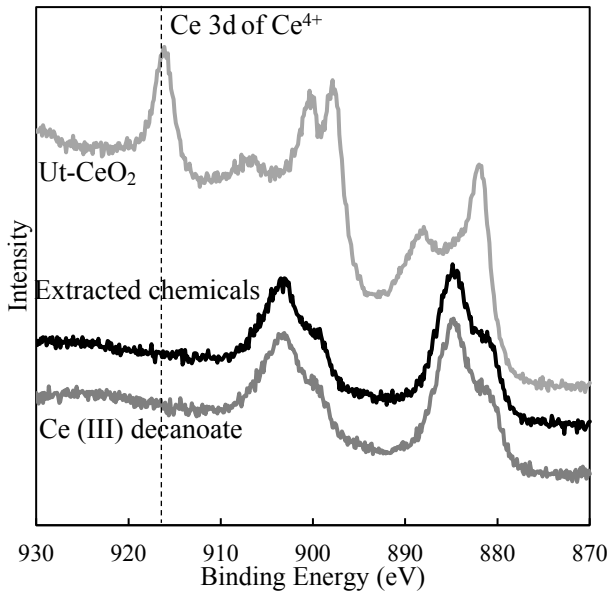

Figure 8. XPS spectra of the Ce (III) decanoate, extracted chemicals, and untreated-CeO_2 (Ut-CeO_2).

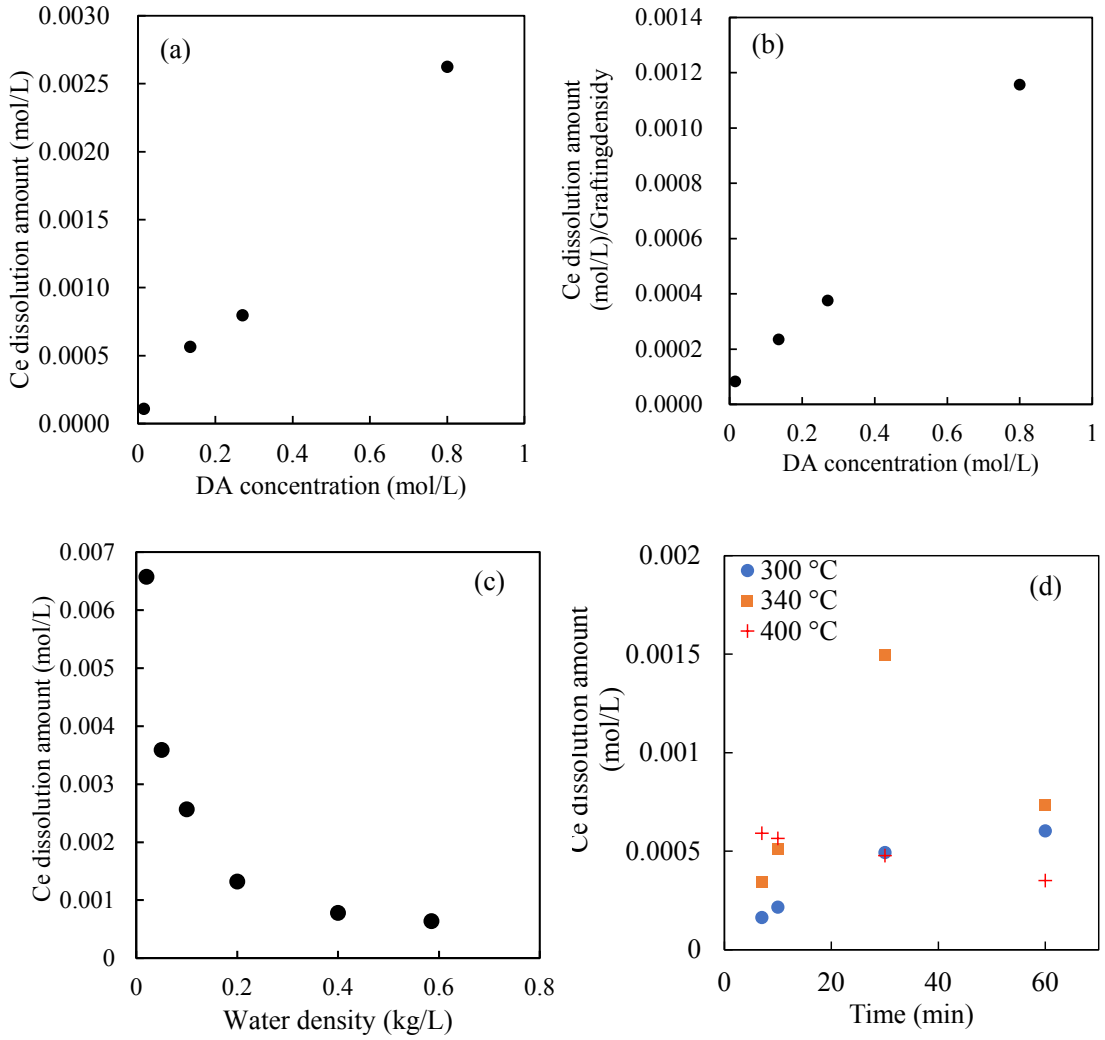

Figure 9. Ce dissolution amounts as complexes calculated by ICP-AES Ce ion concentrations of benzene–methanol supernatant.

(a) Effects of DA concentration on the Ce dissolution amount in the 1 L reaction field.

0.05 mol/L CeO_2, 400 °C, and 0.5 kg/L water density for 10 min.

(b) Ce dissolution amount deducted by grafting density at each DA concentration.

(c) Effects of water density on the Ce dissolution amount in the 1 L reaction field.

0.16 mol/L DA concentration, 0.06 mol/L CeO_2 concentration, and 380 °C for 10 min.

(d) Effects of temperature and treatment time on CeO_2 dissolution amounts in the 1 L reaction field.

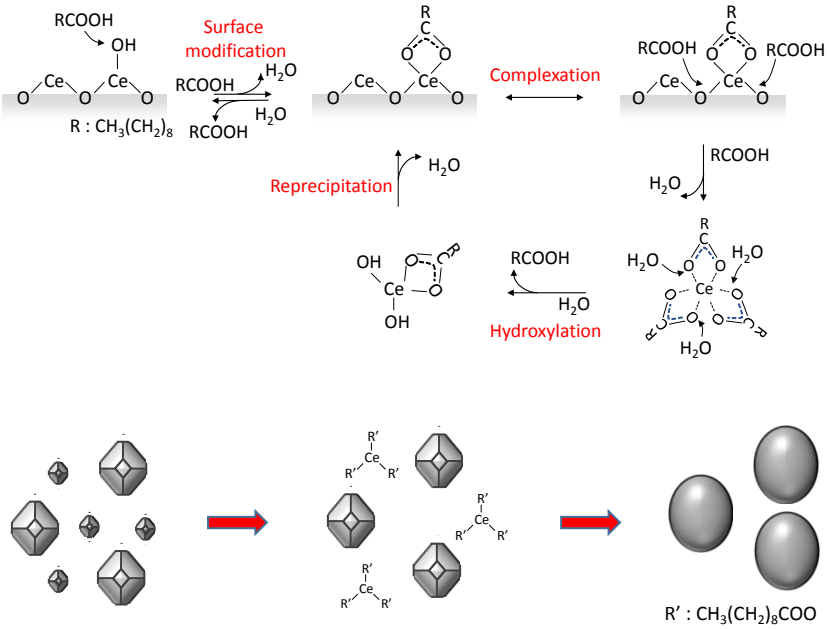

Scheme 1. Proposed mechanism of the Ostwald ripening process promoted by carboxylic acid and water.